White organic light emitting diodes with enhanced internal and external outcoupling for ultra-efficient light extraction and Lambertian emission

Tobias Bocksrocker,[1,*] Jan Benedikt Preinfalk,[1] Julian Asche-Tauscher,[1] Andreas Pargner,[1] Carsten Eschenbaum,[1] Florian Maier-Flaig,[1] Uli Lemmer[1]

[1]*Light Technology Institute, Karlsruhe Institute of Technology (KIT), Kaiserstr. 12, D-76131 Karlsruhe, Germany*
[*]*tobias.bocksrocker@kit.edu*

Abstract: White organic light emitting diodes (WOLEDs) suffer from poor outcoupling efficiencies. The use of Bragg-gratings to enhance the outcoupling efficiency is very promising for light extraction in OLEDs, but such periodic structures can lead to angular or spectral dependencies in the devices. Here we present a method which combines highly efficient outcoupling by a TiO$_2$-Bragg-grating leading to a 104% efficiency enhancement and an additional high quality microlens diffusor at the substrate/air interface. With the addition of this diffusor, we achieved not only a uniform white emission, but also further increased the already improved device efficiency by another 94% leading to an overall enhancement factor of about 4.

OCIS codes: (230.3670) Light-emitting diodes; (250.3680) Light-emitting polymers; (230.7390) Waveguides, planar; (050.1950) Diffraction gratings.

References and links

1. M. C. Gather, A. Köhnen, and K. Meerholz, "White Organic Light-Emitting Diodes," Adv. Mater. (Deerfield Beach Fla.) **23**, 33–248 (2010).
2. S. Reineke, F. Lindner, G. Schwartz, N. Seidler, K. Walzer, B. Luessem, and K. Leo, "White organic light-emitting diodes with fluorescent tube efficiency," Nature **459**, 234–238 (2009).
3. C. Adachi, M. Baldo, M. Thompson, and S. Forrest, "Nearly 100% internal phosphorescence efficiency in an organic light-emitting device," J. Appl. Phys. **90**(10), 5048–5505 (2001).
4. N. Chopra, J. Lee, J. Xue, and F. So, "High-Efficiency Blue Emitting Phosphorescent OLEDs," IEEE Trans Electron. Dev. **57**, 101–107 (2010).
5. S. O. Jeon, S. E. Jang, H. S. Son, and J. Y. Lee, "External Quantum Efficiency Above 20% in Deep Blue Phosphorescent Organic Light-Emitting Diodes," Adv. Mater. (Deerfield Beach Fla.) **23**(12), 1436–1441 (2011).
6. H. Greiner, "Light Extraction from Organic Light Emitting Diode Substrates: Simulation and Experiment," Jpn. J. Appl. Phys. **46**(7A), 4125–4137 (2007).
7. H. Kim, C. M. Gilmore, A. Piqué, J. S. Horwitz, H. Mattoussi, J. Murata, Z. H. Kafafi, and D. B. Chrisey, "Electrical, optical, and structural properties of indium-tin-oxide thin films for organic light-emitting devices," J. Appl. Phys. **86**(11), 6451–6461 (1999).
8. K. Saxena, V. K. Jain, and D. S. Mehta, "A review on the light extraction techniques in organic electroluminescent devices," Opt. Mater. **32**(1), 221–233 (2009).
9. N. Patel, S. Cina, and J. Burroughes, "High-efficiency organic light-emitting diodes," IEEE J. Sel. Top. Quantum Electron. **8**(2), 346–361 (2002).
10. J. Zhou, N. Ai, L. Wang, H. Zheng, C. Luo, Z. Jiang, S. Yu, Y. Cao, and J. Wang, "Roughening the white OLED substrate's surface through sandblasting to improve the external quantum efficiency," Org. El. **12**(4), 648–653 (2011).
11. J. Shiang, T. Faircloth, and A. Duggal, "Experimental demonstration of increased organic light emitting device output via volumetric light scattering," J. Appl. Phys. **95**(5), 2889–2895 (2004).
12. Y. Sun and S. R. Forrest, "Organic light emitting devices with enhanced outcoupling via microlenses fabricated by imprint lithography," J. Appl. Phys. **100**(7), 073106 (2006).
13. K. H. Liu, M. F. Chen, C. T. Pan, M. Y. Chang, and W. Y. Huang, "Fabrication of various dimensions of high fill-factor micro-lens arrays for OLED package," Sens. and Act. A. **159**, 126–134 (2010).

14. B. Riedel, J. Hauss, M. Aichholz, A. Gall, U. Lemmer, and M. Gerken, "Polymer light emitting diodes containing nanoparticle clusters for improved efficiency," Org. Electron. **11**(7), 1172–1175 (2010).
15. Y. Sun and S. Forrest, "Enhanced light out-coupling of organic light-emitting devices using embedded low-index grids," Nat. Photonics **2**(8), 483–487 (2008).
16. W. H. Koo, S. M. Jeong, F. Araoka, K. Ishikawa, S. Nishimura, T. Toyooka, and H. Takezoe, "Light extraction from organic light-emitting diodes enhanced by spontaneously formed buckles," Nat. Photonics **4**(4), 222–226 (2010).
17. T. Bocksrocker, F. Maier-Flaig, C. Eschenbaum, and U. Lemmer, "Efficient waveguide mode extraction in white organic light emitting diodes using ITO-anodes with integrated MgF$_2$-columns," Opt. Express **20**(6), 6170–6174 (2012).
18. U. Geyer, J. Hauss, B. Riedel, S. Gleiss, U. Lemmer, and M. Gerken, "Large-scale patterning of indium tin oxide electrodes for guided mode extraction from organic light-emitting diodes," J. Appl. Phys. **104**(9), 093111 (2008).
19. B. Riedel, J. Hauss, U. Geyer, J. Guetlein, U. Lemmer, and M. Gerken, "Enhancing outcoupling efficiency of indium-tin-oxide-free organic light-emitting diodes via nanostructured high index layers," Appl. Phys. Lett. **96**(24), 243302 (2010).
20. J. Hauss, T. Bocksrocker, B. Riedel, U. Lemmer, and M. Gerken, "Metallic Bragg-gratings for light management in organic light-emitting devices," Appl. Phys. Lett. **99**(10), 103303 (2011).
21. J. Lupton, B. Matterson, I. Samuel, M. Jory, and W. Barnes, "Bragg scattering from periodically microstructured light emitting diodes," Appl. Phys. Lett. **77**(21), 3340–3342 (2000).
22. J. Ziebarth, A. Saafir, S. Fan, and M. McGehee, "Extracting light from polymer light-emitting diodes using stamped Bragg gratings," Adv. Funct. Mater. **14**(5), 451–456 (2004).
23. M. Fujita, K. Ishihara, T. Ueno, T. Asano, S. Noda, H. Ohata, T. Tsuji, H. Nakada, and N. Shimoji, "Optical and electrical characteristics of organic light-emitting diodes with two-dimensional photonic crystals in organic/electrode layers," Jpn. J. Appl. Phys. **44**(6A), 3669–3677 (2005).
24. J. Hauss, T. Bocksrocker, B. Riedel, U. Lemmer, and M. Gerken, "On the interplay of waveguide modes and leaky modes in corrugated OLEDs," Opt. Express **19**(S4 Suppl 4), A851–A858 (2011).

1. Introduction

White organic light emitting diodes (WOLEDs) are considered to be a very promising candidate for future lighting applications. A further enhancement of the device efficiency is of pivotal importance to enable commercialization of this revolutionary illumination technology. Recent progresses in materials and device architectures were important steps for achieving this goal [1,2]. Even though high internal quantum efficiencies can be achieved [3–5], external quantum efficiencies in OLEDs are much smaller due to the incomplete light extraction. Since the organic layers and the typically used ITO anode have an overall thickness of about 200 nm and feature high refractive indices in the range of 1.7 – 2.1 [6,7], an organic light emitting diode (OLED) forms a slab waveguide. OLEDs are usually built on glass substrates with a refractive index of about 1.5. Therefore, optical losses due to waveguide modes and surface plasmon polaritons (about 50% of the generated light) and total internal reflection at the substrate/air interface (about 30% of the generated light) add up and lead to extraction efficiencies of only 20% in standard devices [8,9].

The optical losses due to substrate modes can be reduced via roughening the surface (e.g. via sandblasting) [10], by the use of nanoparticles as scattering medium [11] or through microstructures [12,13]. The extraction of waveguide modes is challenging, as one has to alter the OLED-stack itself, potentially causing changes of the internal optoelectronic device characteristics. The use of nanoparticles as scattering centers or the integration of internal Bragg grating lead to an enhanced internal outcoupling but also cause changes of the electrical behavior of the devices [14]. The integration of microcstuctures for outcoupling reduce the active area of the devices and are demanding in terms of the fabrication [15,16]. Recently, we have elaborated a feasible pathway for microstructuring the anode for improving the extraction efficiency in WOLEDs without changing the electrical behavior of the devices [17]. The observed enhancement by a factor of about 1.4 however, is expected to be surpassed by the use of internal diffractive nanostructure which leads to a stronger outcoupling. Periodic nanostructures have been integrated in monochrome devices [18–22] to enhance the outcoupling. The enhancement factors achieved however did not reach the optimum as a high contrast in the refractive indices between the grating and the surrounding is needed for high extraction efficiencies. In this report we have used a high index material to

optimize the extraction. However, Bragg-gratings lead to a high angular dependence of the emission spectrum [18–20]. This is a serious drawback for both, illumination and display applications. This issue becomes even more relevant in the case of white OLEDs which are expected to emit in a Lambertian manner without any visible color shift. Here we demonstrate the combination of a high-index Bragg grating with a well-adjusted microlens array acting as an outcoupling and diffusing structure. We report the use of Bragg-gratings consisting of TiO_2 in white OLEDs, fabricated by laser interference lithography. By adjusting the grating height and period we achieve an efficiency enhancement by a factor of more than 2. In order to suppress the angular and spectral dependency, we use a high quality microlens array as a diffusor at the substrate/air interface. This not only results in a uniform emission of the WOLEDs, but also increases the efficiency of the already improved device by almost another factor of 2. The total enhancement factor of ~4 is achieved by using two upscalable low cost processes.

2. Fabrication

2.1 Bragg-grating fabrication

As a substrate we use ITO-covered glass with a size of 25 mm x 25 mm. The ITO of the substrates was pre-patterned for contacting, such that each substrate contained four active areas, each with a size of 5 mm x 5 mm. The substrates were subsequently cleaned with acetone and isopropyl alcohol in an ultrasonic bath for 10 min. After cleaning, the ITO-substrates were treated with oxygen plasma for 2 min. The substrates were then covered with a monolayer of hexamethyldisilazane (HMDS) as an adhesive for the photoresist. The photoresist AR-P 3170 (purchased from Allresist) was then spincast at 3000 rpm for 20 s resulting in a ~500 nm layer. After curing the resist for 60 s at 80°C we started to fabricate the grating structures on the substrates. We used a laser interference setup as depicted in Fig. 1(a). As a laser source we used a solid state laser (FQCW 266-50/100 from CryLas GmbH) with a wavelength of 266 nm. The laser beam was split into two separate beams which were then widened up with standard UV-lenses. The beams were brought to interference at the sample surface. The optical power on the substrate surface was monitored with a photodiode close to the sample. By changing the incident angle θ of the beams the resulting grating period Λ can be adjusted according to $\Lambda = \dfrac{\lambda}{\sin \theta}$, with λ being the wavelength of the laser.

The photoresist was exposed to the interference pattern resulting after development of the substrates in a photoresist grating, see Fig. 1(b). We then evaporated a layer of TiO_2 on the resist grating (Fig. 1(c)) and then performed a lift-off with acetone leaving a negative of the resist grating on the substrate (Fig. 1(d)). Figure 1(e) shows a SEM-image of a resulting TiO_2 grating with a period of 330 nm.
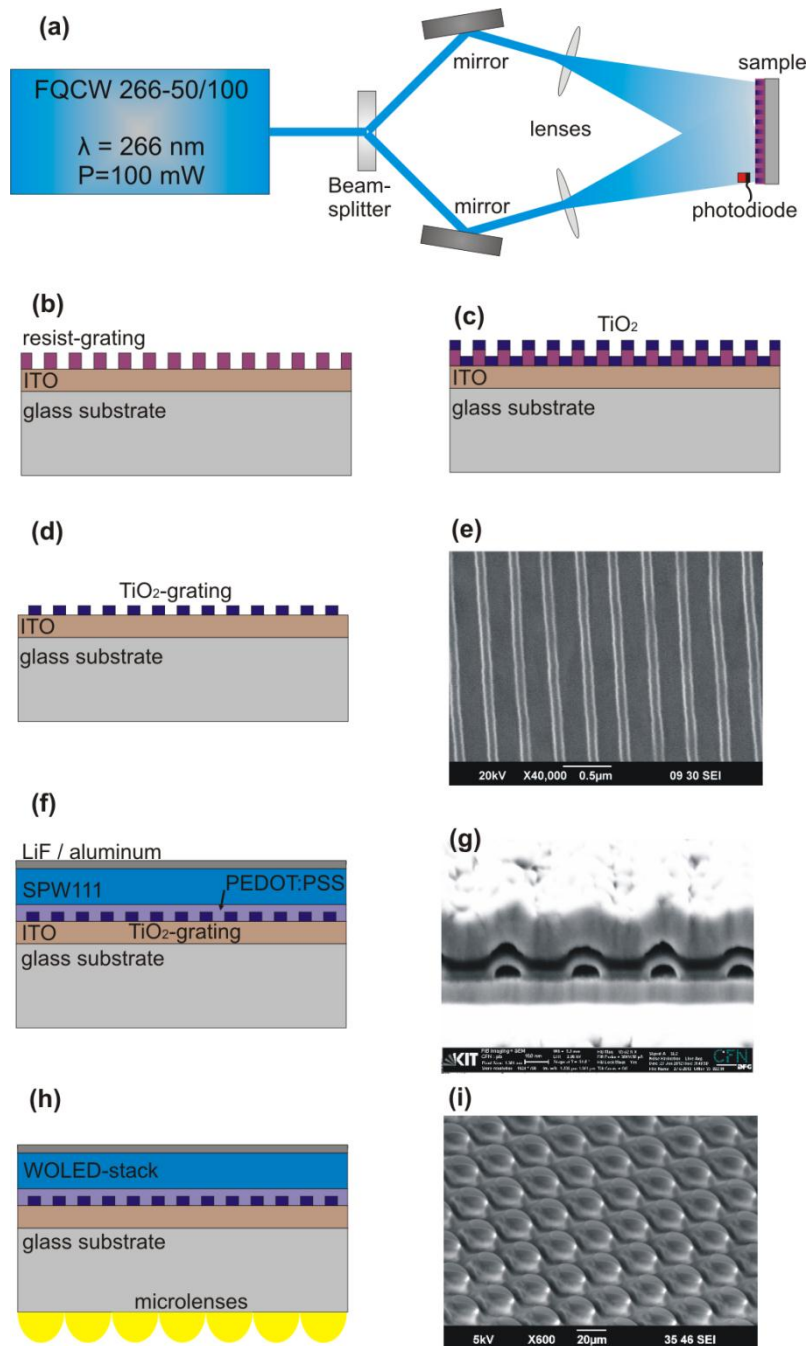
Fig. 1. Fabrication schemes: (a) Laser-interference lithography setup. The laser beam is split into two separate beams, which are widened up and are brought to interference under a certain angle at the substrate surface. (b) After illumination the resist is developed, which leaves a resist grating on the sample. (c) TiO_2 is evaporated onto the sample. (d) After lift-off a TiO_2 grating results. (e) SEM image of a TiO_2 grating with a 330 nm period. (f) The WOLED stack is fabricated on top. (g) SEM image of a cross section of a finished WOLED with grating. (h) A PDMS microlens stamp is pressed into a layer of PMMA/anisol, which results into a microlens array at the substrate/air interface. (i) SEM image of a microlens array.

2.2 WOLED fabrication

The WOLED-stack was fabricated on top of the ITO-covered substrate containing the TiO_2 grating (Fig. 1(f)). For the reference devices, the same ITO-covered substrates were used, but without the grating structure. All substrates where cleaned again with acetone and isopropyl alcohol in an ultrasonic bath and treated again with oxygen plasma for 2 min. All WOLEDs were fabricated under nitrogen atmosphere to avoid any degradation of the organic materials. The WOLED-stack was fabricated from solution. Poly(3,4-ethylenedioxythiophene):poly(styrenesulfonate) (PEDOT:PSS, Baytron P VPAI 4083) was diluted with H_2O in a 1:1 ratio and then spincoated at 4000 rpm on the substrates resulting in a ~20 nm thick layer. For the emissive layer we used a white co-polymer (SPW111 from Merck OLED Materials GmbH) in a 6 mg/ml toluene solution, spincoated at 1000 rpm for 55 s resulting in a ~70 nm thick layer. As a cathode we evaporated a lithium fluoride (1 nm) and an aluminum (200 nm) layer under vacuum (10^{-7} mbar). To operate the devices under ambient atmosphere, the devices were then encapsulated with an epoxy adhesive and a glass cover.

2.3 Fabrication of the microlens arrays

We have developed a versatile approach which allows easy tuning of the size, the diameter and the aspect ratio of the microlens arrays. A 25 µm thick SU-8 layer was spincoated on a silicon wafer. The resist was illuminated with a shadow mask, such that after a post bake and development of the resist circular columns with a diameter of 30 µm and a gap of 6 µm resulted in a hexagonal array on the wafer. Those columns were molded into polydimethylsiloxane (PDMS). After hardening the PDMS was removed, leaving the negative of the columns in an intermediate PDMS tool. This PDMS negative was used to stamp the columns into a gel-like layer of poly(methyl methacrylate) (PMMA) and anisol on a glass substrate. After the PMMA solidified, the PDMS stamp was removed. The remaining PMMA columns were baked at 250°C for 150 s, leading to a reflow of the columns which resulted in microlenses with a height of ~18µm and a very high packing density, meaning the pitch is basically the same as the resulting microlens diameter (~33 µm). These master arrays were replicated again to result in a PDMS tool. This tool was then used to stamp the arrays into a PMMA/anisol layer on the backside of the OLEDs (Fig. 1(g)), leading to a rapid replication of the microlens arrays on the backside of the WOLEDs. A scheme of resulting device is depicted in Fig. 1(h). An SEM-image of the high quality microlens array is shown in Fig. 1(i).

3. Measurement and results

The overall efficiencies of the devices were compared with an integrating sphere, without collecting the edge emission of the OLEDs. As a power supply and for monitoring the IV-characteristics of the WOLEDs we use a source measure unit (Keithley SMU 236). A multimode fiber is coupled from the integrating sphere to a spectrometer (Acton Research Corporation SpectraPro-300i) with an attached ICCD-camera (Princeton Instruments PiMax:512). The used goniometric setup to record the angle resolved spectral emission of the devices, consists of a multimode fiber that is connected to the same spectrometer. In this setup the WOLEDs are driven by a constant current (at 5 mA/cm^2, see also Fig. 2(a)), and then rotated with respect to the fiber. Thus the emission spectra for different viewing angle are recorded.

With the Bragg scattering equation $\theta = \arcsin\{n_{eff} \pm m \cdot \frac{\lambda_0}{\Lambda}\}$, n_{eff} being the effective refractive index and m being the order of scattering, we calculated the necessary period for the grating, such that the guided modes scatter via first order processes into the escape cone (see Fig. 3(a)) for the complete visible spectrum. This condition is fulfilled for a period of Λ = 330 nm.

In the following, we compare the measured optoelectronic properties of the devices with two different grating heights (35 nm and 15 nm) and compare each device with and without a microlens array. Figure 2(a) shows the I-V characteristics of the devices. The structured devices all show a slight shift towards higher current densities, which can be explained by the field enhancement resulting from the corrugated layers [19,23]. Even though the devices were solution processed, this did not completely smoothen the corrugation resulting from the grating structure (see Fig. 1(g)). To investigate possible electrical effects on the device efficiencies due to corrugation, Fig. 2(b) shows the relative current efficiency of the devices without the microlens arrays. By comparison to the relative power efficiency in Fig. 2(c) we attribute the enhancement mostly to an optical effect, since both quantities show a significant enhancement.
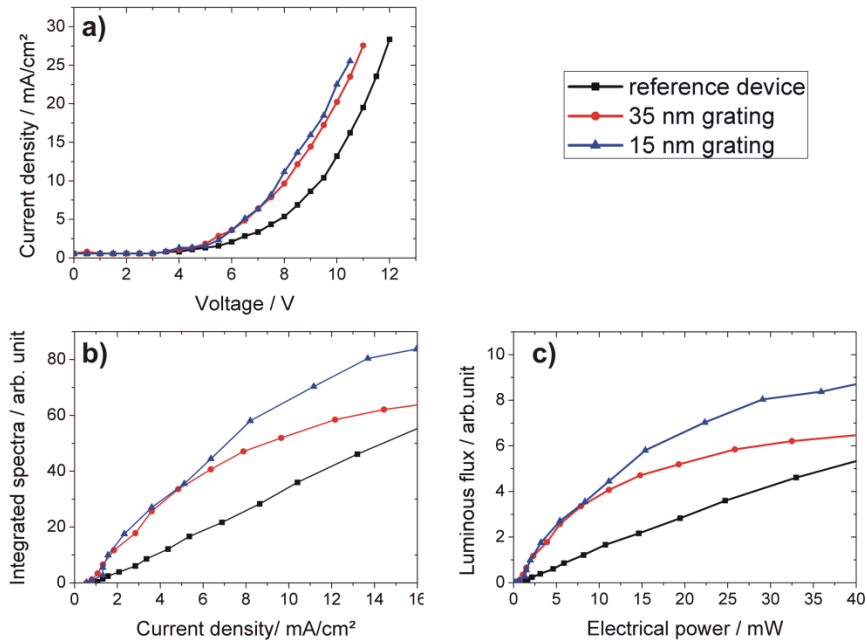

Fig. 2. (a) Measured I-V characteristics of the reference device and the devices with 15 nm and 35 nm grating height. (b) Relative current efficiencies of the devices. (c) Relative power efficiencies of the devices.

First we compare the relative power efficiencies of the grating structured devices without microlenses at a reference device luminance of ~300 cd/m^2 (which correlates to a power consumption of 25 mW). For higher or lower power consumptions the discussed enhancement factors can be slightly different. For the same power density the device with 15nm gratings shows an efficiency enhancement of 104% ($\pm$ 5%), while the device with a 35 nm grating results in an increase of 59% ($\pm$ 4%), see Fig. 2(c). These findings are in agreement with recent results in [24] where we discussed the complex interplay of scattering processes between waveguide modes, substrate modes and radiation modes. For certain geometries the losses due to enhanced *in*coupling of radiation modes into waveguide modes might overcompensate the enhanced *out*coupling of waveguide modes into radiation modes. The scheme in Fig. 3(b) illustrates the different scattering processes. In our devices the outcoupling is more dominant for both grating thicknesses, but with the 15 nm grating device the back-coupling seems to be smaller than in the 35 nm grating device. Therefore the amount of the extracted photons is higher with this device.
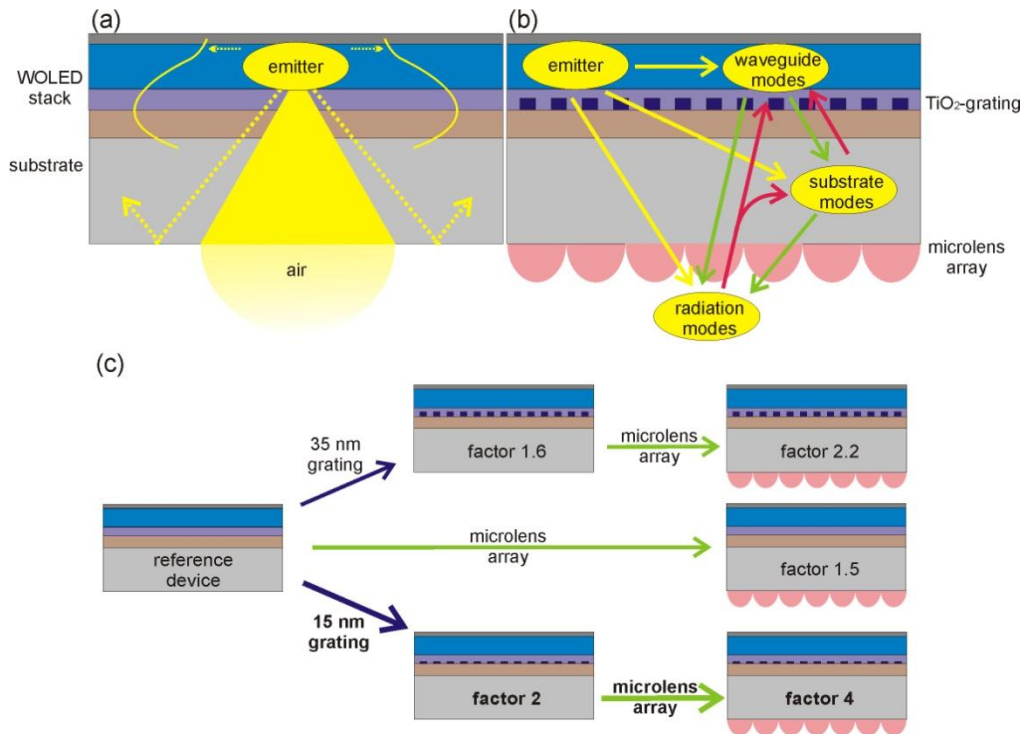
Fig. 3. (a) Scheme of light propagation in the reference device. Generated light is partly trapped in waveguide modes and in substrate modes. Light in the escape cone has the chance to exit the device (radiation modes). (b) Possible scattering of photons due to the grating. Yellow arrows: the emitter couples to waveguide modes, substrate modes and radiation modes. Green arrows: the grating can scatter waveguided photons to substrate modes and radiation modes. Photons that were initially in substrate modes can also scatter into radiation modes. Red arrows: back scattering of photons from radiation modes or substrate modes into waveguide modes. Photons from radiation modes can also scatter into substrate modes. (c) Overview off the different devices and their respective enhancement factors.

By adding the microlens arrays we can significantly enhance the efficiency of the already improved devices. In case of our 15 nm grating device, the relative efficiency enhancement, as shown in Fig. 4(a) of the grating WOLED is 94% (± 4%), leading to a total enhancement factor of about 4 compared to the completely unstructured reference device. The 35 nm grating device was also improved (see Fig. 4(b), but only by 35% (± 3%). For the reference device without a grating we observe an enhancement of 50% (± 4%). Our results are in agreement with the notion that depending on the used grating, more or less light is trapped in the glass substrate (see Fig. 3(b)). Consequently, the microlens arrays can affect more or less light in substrate modes. This indicates that the grating height not only influences the outcoupling of waveguide into radiation modes but also the in- and outcoupling of substratemodes into radiation and waveguide modes. The overall efficiency enhancement factor of ~4 indicates a high outcoupling efficiency for the combination of the 15 nm grating with the microlens array. Figure 3(c) gives an overview off the different enhancement factors achieved by the grating devices, the microlens arrays and their combination.
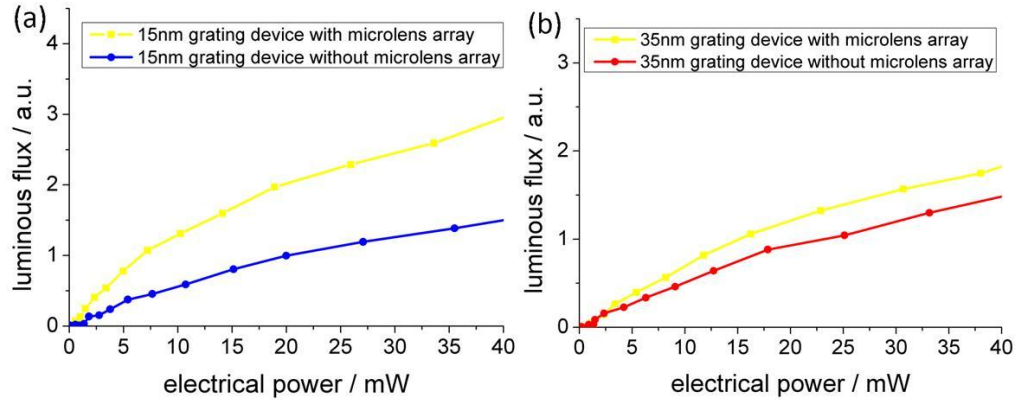
Fig. 4. (a) Comparison of the relative efficiencies of the 15 nm grating device with and without the microlens array. (b) Relative efficiencies of the 35 nm grating device with and without the microlens array.

Figures 5(a)-5(d) show the angle resolved emissions spectra of our devices. The viewing angle of 0° is perpendicular to the luminous area (frontal view). The comparison of the 35 nm grating device (Fig. 5(a)) and the 15 nm grating device (Fig. 5(c)) without additional microlenses show, that the grating induced spectral features get stronger for the larger grating height. The grating features in the angle resolved spectral emission for the 15 nm grating device are smaller, but the efficiency enhancement is significantly larger than with the 35 nm grating device (see Fig. 4(a)-Fig. 4(b)). This can be explained by the interplay of the in- and outcoupling through the grating.

An angle independent white light emission is achieved when a microlens array is added. Figures 5(b) and 5(d) depict the angle resolved spectral emission of the very same devices as in Figs. 5(a) and 5(c) respectively, but with the microlens arrays as a diffusing and outcoupling layer. The grating features vanish and hence the WOLEDs show a uniform white emission. It is clearly evident, that the emission is diffused by the microlens array.
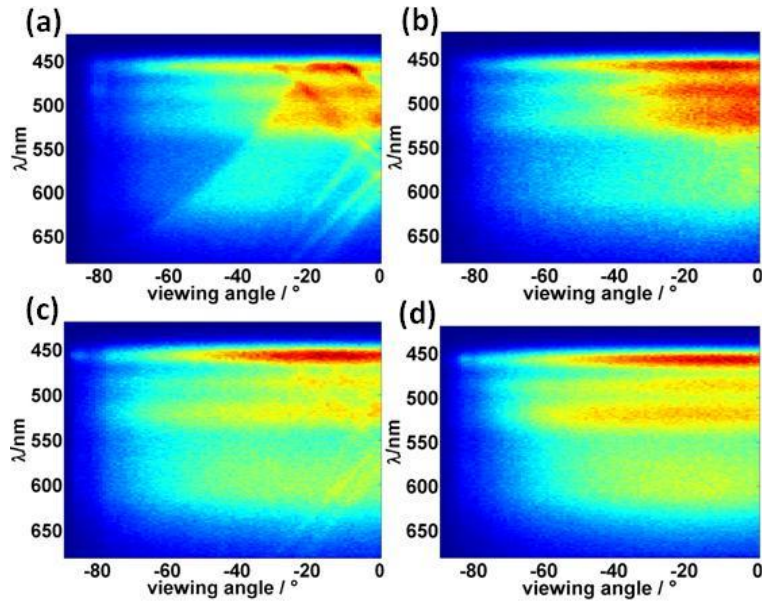
Fig. 5. (a)-(d) Measured angle resolved normalized spectral emission of the same luminous areas. The 35 nm grating device without (a) and with (b) the microlens array and the 15 nm grating device without (c) and with (d) the microlens array.

Furthermore, the microlens arrays reduce the total internal reflection at the substrate/air interface as described above. We emphasize, that all measurements have been performed on the very same devices. After measuring the devices with the microlens arrays we removed the arrays by simply peeling them off and performed the measurement again.

4. Conclusion

In conclusion we have presented a method to optimize the outcoupling efficiency and viewing angle of WOLEDs. By adding a high index Bragg-grating consisting of TiO_2 into the WOLED stack and adjusting the grating height we were able to achieve an overall efficiency enhancement of up to 104%. By adding a high quality microlens array we were able to enhance the efficiency of the already improved devices by another 94%, leading to an overall enhancement factor of ~4. Furthermore, the microlens array diffuses the emitted light, leading to a uniform white emission with no angular or spectral dependencies.